Reliability Engineering and System Safety 000 (2018) 1–11

Contents lists available at ScienceDirect

Reliability Engineering and System Safety

journal homepage: www.elsevier.com/locate/ress

Time and magnitude monitoring based on the renewal reward process

Sajid Ali [a,b,*], Antonio Pievatolo [c]

[a] Department of Statistics, Quaid-i-Azam University, Islamabad 45320, Pakistan
[b] Department of Decision Sciences, Bocconi University, via Röentgen 1, Milan 20136, Italy
[c] CNR-IMATI, via Bassini 15, Milan 20133, Italy

ARTICLE INFO

MSC:
62P30
60K05
60K10
60K30
62L99

Keywords:
Average run length (ARL)
Compound poisson process
High-quality process
Renewal reward processes
Time-between-events control chart
Time and magnitude monitoring

ABSTRACT

Time between event (TBE) charts are SPC tools for monitoring the occurrence of unwanted events, such as the appearance of a defective item or a failure of a piece of equipment. In some cases, a magnitude, indicating the severity of the event, is also measured. Time and magnitude charts, which are based on the assumption that the stochastic process underlying the occurrence of events is the marked Poisson process, are the preferred option. However, these charts are not suitable to deal with damage events caused by repeatedly occurring shocks or stress conditions. To bridge this gap, we introduce a new control chart based on the assumption of a renewal process with rewards, where the reward represents magnitude, and a magnitude-over-threshold condition represents the occurrence of an event. In particular, we consider two cases for magnitude: (i) magnitude is cumulative over time and (ii) magnitude is non-cumulative or independent over time. We use known results in renewal theory to provide expressions of the probability distributions needed to compute the control limits and perform a simulation analysis of the control chart performance.

1. Introduction

Statistical quality control is a collection of statistical methods, which are used to monitor and improve the quality of a process. Currently, statistical quality control is not limited to the manufacturing industry, but is also used in environmental science, biology, genetics, epidemiology, medicine, finance, law enforcement and athletics. Among the SPC tools, control charts are probably the most technically sophisticated. One of the main purposes of control charts is to distinguish between the variation due to chance causes and the variation due to assignable causes in order to prevent overreaction and under-reaction to the process (cf. [1]).

There are different types of control charts in the literature to handle different situations [2]. A special type of control chart called time-between-events (TBE) is used to monitor rare events or the so-called high-quality processes. Traditional TBE charts considered the time interval X between the occurrences of an event by completely ignoring the magnitude M associated with it, representing the size of the event itself. However, there are many real applications where both time and magnitude are important and ignoring one of them leads to misleading conclusions. If the magnitude is also available, it has been recognised that a joint monitoring of time and magnitude improves the performance of the control chart. For example, Wu et al. [3] proposed control charts for the combined monitoring of TBE and magnitude, providing a decision rule based on both individual X and M charts. Later, Wu et al. [4] introduced the rate chart to monitor magnitude and TBE data by considering their ratio, finding that it is more effective than the individual X or M charts and also than the combined monitoring chart. The rate chart with an integer magnitude was proposed by Liu et al. [5]. Liu et al. [6] proposed a joint control chart by considering a truncated Poisson distribution for the magnitude, finding that the new chart outperforms the individual charts. Recently, Qu et al. [7] also introduced a time and magnitude chart by assuming an exponential distribution for time and a normal distribution for magnitude. The authors compared the proposed chart with the existing ones, i.e., time, magnitude, time and magnitude, and rate charts, and showed that the new chart is more efficient. Some works related to CUSUM charts are Wu et al. [8], Qu et al. [9], and Qu et al. [10]. We refer to Ali et al. [11] for a detailed review about time and magnitude control charts.

The importance of control charts for reliability data has been highlighted by Xie et al. [12]. More recently, Vining et al. [13] observed that there is a need to develop process control techniques for reliability data to ensure that a product or a process maintains the expected reliability standard. In this paper we are concerned with damage events caused by randomly occurring shocks or stress conditions, which eventually lead to a failure event or require repair when the magnitude of the damage has

* Corresponding author at: Department of Statistics, Quaid-i-Azam University, Islamabad 45320, Pakistan.
E-mail addresses: sajidali@qau.edu.pk (S. Ali), antonio.pievatolo@mi.imati.cnr.it (A. Pievatolo).

https://doi.org/10.1016/j.ress.2018.01.004
Available online xxx
0951-8320/

crossed an appropriate threshold. This event can be categorized into two failure modes: catastrophic failure, in which the failure occurs by some sudden shock, and cumulative shock failure, in which the failure occurs by physical deterioration due to age or cumulative wear. The two cases will be called *independent damage process* and *cumulative damage process*, respectively. The renewal process with rewards is suitable to describe both, by considering as the time for the occurrence of an event the first passage time above the threshold either by a single reward or by the accumulated rewards. When a magnitude-over-threshold event happens, the product or process are renewed and the next TBE is the next first passage time, so that this chart can be called an FPT-chart. By monitoring this TBE, a reliability engineer can assess whether a product is being used according to its design limits or a process is being run according to specifications. A too frequent occurrence of magnitude-over-threshold events could also indicate deficiencies in the material used for the product or for the equipment involved in the process. A simple example of an independent damage process and of cumulative damage process is provided by Gut and Hüsler [14]: a material, such as a rope or a wire, can break due to fatigue because of the cumulative effect of loads within design limits after a long period of time or because a sudden big load exceeding its capacity; capacity could as well be lower than expected due to faulty material.

The existing time and magnitude control charts are based on the marked Poisson process, although this is not always explicitly stated. The renewal reward assumption is a generalisation in the direction of any lifetime distribution for the occurrence of shocks. However, time and magnitude charts monitor every single magnitude and TBE, not first passage times, therefore the FPT-chart cannot be viewed as a direct generalisation, rather as a complement to these. For example, if the magnitude is not directly observable and a shock process is in effect (be it independent or cumulative), then the failure time is a first passage time and it has a non-exponential distribution even in the simplest settings. In this case time and magnitude charts cannot be applied, while the FPT-chart is still usable because it is not necessary to establish a threshold to observe failures. If the magnitude is observable, both charts can be applied, but they are expected to react differently to the same changes in the underlying process. In case of a zero threshold the FPT-chart is a simple TBE chart.

This study is organized as follows. In Section 2 we define the renewal reward process formally and provide expressions for the first passage time distributions. The compound Poisson process is also mentioned as a special case of the renewal reward process. The FPT-chart construction and a numerical study of performance measures are given in Section 3. Also, a comparison of FPT charts with rate charts is presented in Section 3. An implementation of the FPT-chart is the subject of Section 4. Section 5 contains a brief summary of the outcomes, conclusions and suggestion for future studies.

2. Cumulative and independent processes

In this section, we shall introduce the necessary definitions and formulas that are required for the development of FPT-charts, obtained from Nakagawa [15] and Nakagawa [16].

We denote by $N(t)$ a counting process, by X_i the TBE and by M_i the magnitude associated with X_i for $i \geq 1$.

Definition 2.1. A counting process $\{N(t),\ t \geq 0,\ t \in T\}$ with independent and identically distributed (iid) inter-arrival times $X_1, X_2, \ldots$ with a common distribution F is called a renewal process.

Definition 2.2. Let $N(t)$ be a renewal process and let M_i denote the reward (such as damage, wear, fatigue, or cost) that is attached to each inter-arrival time X_i. If the pairs (X_i, M_i) for $i = 1, 2, \ldots$ are independent and identically distributed, then the stochastic process $Y(t) = \sum_{i=1}^{N(t)} M_i$ is called a renewal reward process.

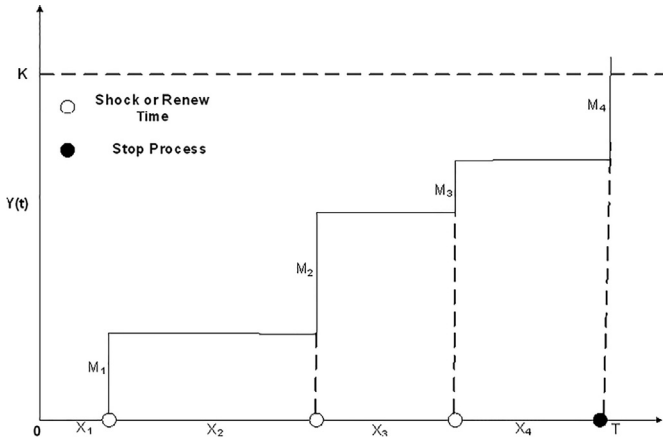

Fig. 1. Process for a standard cumulative damage model.

Therefore, the renewal reward assumption is a generalization of the marked Poisson process.

Let $F(x) = Pr\{X_i \leq x\}$ and $G(m) = Pr\{M_i \leq m\}$ be the cumulative distribution functions of X_i and M_i, respectively, with finite means. In addition, suppose K is a fixed threshold for the damage. In the cumulative damage scenario, the FPT-chart is based on the distribution of Z, the first passage time: $Pr\{Z \leq t\}$ where $Z = \min_t\{Y(t) > K\}$. For the independent damage scenario, the first passage time can be defined as $Z = \sum_{j=1}^{i^*} X_j$, where $i^* = \min\{j = 1, 2, 3, \ldots | M_j > K\}$. We remark that K can be only implied if the damage due to shocks is not observable and Z represents the time of an observable failure.

In the following subsections we provide expressions for the distribution of Z, including also the homogeneous compound Poisson process, as a special case of the renewal reward process.

2.1. Cumulative damage process

Definition 2.1.1. Let $(X_i,\ M_i)$ denote a sequence of times between shocks (X_i) with an associated damage (M_i) undergone by a unit or system. Suppose that each damage is additive and the system or unit fails when the total damage has exceeded a failure threshold K where $0 < K < \infty$, for the first time (cf. Fig. 1). A process with such a behavior is called a cumulative damage process.

If $Y(t)$ is a renewal reward process, then the distribution of the first passage time Z is

$$\phi(t) = Pr\{Z \leq t\} = \sum_{n=0}^{\infty} [G^{(n)}(K) - G^{(n+1)}(K)] F^{(n+1)}(t)\ . \tag{1}$$

2.2. Independent damage process

Definition 2.2.1. Let $(X_i,\ M_i)$ denote a sequence of times between shocks (X_i) with an associated damage (M_i) undergone by a unit or system. Suppose that the damage is not additive and the system or unit fails the first time the amount of damage a threshold level K. This type of process is called an independent damage model (cf. Fig. 2).

The first passage time distribution is

$$Pr\{Z \leq t\} = \sum_{n=0}^{\infty} [G^{n}(K) - G^{n+1}(K)] F^{(n+1)}(t)\ . \tag{2}$$

Notice that Eq. (2) does not have the convolution (.) for the magnitude distribution as compared to Eq. (1).

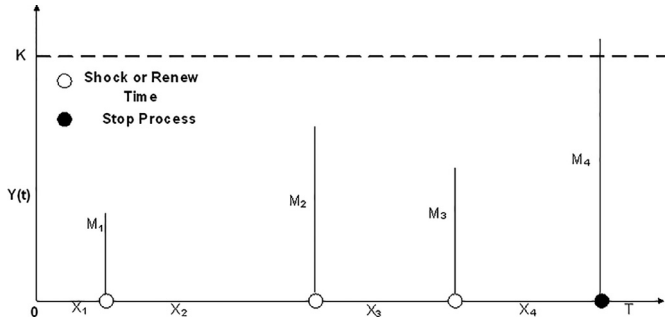

Fig. 2. An illustration of an independent damage model.

2.3. Poisson process

The cumulative and independent damage concepts can also be modelled through a Poisson process assumption for the process driving the TBE, which is a special case of a renewal process.

For the cumulative damage process, a compound Poisson process plays an important role. More specifically, if $N(t)$ is a Poisson process with rate λ, then the counting process $Y(t) = \sum_{i=1}^{N(t)} M_i$, where the M_i's are IID random variables independent of $N(t)$ for $N(t) = 0, 1, 2, \cdots$ and $Y(t) = 0$ when $N(t) = 0$, is called a compound Poisson process. The general formulas for the distribution of the first passage time are special cases of (1) and of (2) where F is an exponential distribution with rate λ. Closed-form expressions can be obtained in this case, as shown in the following examples.

Example#1: Suppose that the time and the damage both have the exponential distribution with mean $1/\lambda$ and $1/\theta$, respectively, i.e., $F(x) = 1 - \exp(-\lambda x)$ and $G(m) = 1 - \exp(-\theta m)$. Then, to derive the first passage distribution for the cumulative process we have to solve $\int_0^\infty \exp(-sm) d\,Pr\{Y \le m\} = \exp(-\lambda t[s/(s+\theta)])$, and its inversion can be written as follows (cf. Barlow and Proschan [17], and Graf [18]):

$$Pr\{Y(t) \le t\} = \exp(-\lambda t)\left[1 + \sqrt{\lambda\theta t}\int_0^x \exp(-\theta w) w^{-0.5} I_1(2\sqrt{\lambda\theta t w}) dw\right] \tag{3}$$

where I_i is the Bessel function of order i for the imaginary argument defined as $I_i(x) = \sum_{k=0}^\infty \frac{(x/2)^{2k+1}}{k!(k+i)!}$. Thus, we have

$$Pr\{Z \le t\} = 1 - \exp(-\lambda t)\left[1 + \sqrt{\lambda\theta t}\int_0^K \exp(-\theta w) w^{-0.5} I_1(2\sqrt{\lambda\theta t w}) dw\right] \tag{4}$$

and $E\{Y(t)\} = \frac{\lambda t}{\theta}, E\{Z\} = \frac{\theta K+1}{\lambda}, Var\{Y(t)\} = \frac{2\lambda t}{\theta^2}$ and $Var\{Z\} = \frac{2\theta K+1}{\lambda^2}$, respectively. It is to be noted that $E\{Y(t)\}$ is increasing linearly with time t and therefore, we have $\frac{E\{Y(t)\}}{K+\theta^{-1}} = \frac{t}{E(Z)}$.

Example#2: The first passage time distribution of the independent damage scenario for the exponentially distributed time and magnitude is:

$$Pr\{Z \le t\} = 1 - \exp(-\lambda t \exp(-\theta K)) \tag{5}$$

which is again an exponential distribution with parameter $\lambda\exp(-\theta K)$. Therefore, we have $E(Z) = \frac{\exp(\theta K)}{\lambda}$ and $Var(Z) = \frac{\exp(2\theta K)}{\lambda^2}$.

In Eq. (5), we have considered the exponential distribution for the magnitude. If we assume a gamma distribution, the real task is to solve the Laplace integral $\int_0^\infty \exp(-sx) d\,Pr\{Y \le x\} = \exp(-\lambda t[1 - (\theta/(s+\theta))^\beta]) = \exp(-\lambda t)\exp(\lambda t(\theta/(s+\theta))^\beta)$. One can write $\exp(\lambda t(\theta/(s+\theta))^\beta)$ as $\sum_{n=0}^\infty \frac{(\lambda t)^n}{n!}\left(\frac{\theta}{s+\theta}\right)^{n\beta}$. Now its Laplace-Stieltjes inversion is $\sum_{n=0}^\infty \frac{(\lambda t)^n}{n!}\left(-n\beta\lambda \times_1 F_1[1+n\beta, 2, -t\lambda]\right)$, where ${}_1F_1$ denotes the Kummer Confluent Hypergeometric function. By comparing this expression with Eq. 5, one can notice that the first passage distribution has become very complicated after replacing the exponential distribution with a gamma.

3. Control chart construction

As illustrated in the preceding sections, the FPT-chart is built using the distribution of the first passage time Z (which is now the TBE for this chart) either with the cumulative damage or the independent damage assumption, as displayed in Figs. 1 or 2. The damage is zeroed after a threshold crossing, so that in-control Z_{i+1} has the same distribution of Z_i.

Let α denote the false alarm probability and let F_Z be the cumulative distribution function of Z. To construct a two-sided control chart the lower control limit (LCL) and the upper control limit (UCL) are calculated as percentiles of F_Z: $LCL = F_Z^{-1}(\alpha/2)$ and $UCL = F_Z^{-1}(1-\alpha/2)$, for the two-sided control chart. For the detection of a process deterioration or of a process improvement only $LCL = F_Z^{-1}(\alpha)$ or $UCL = F_Z^{-1}(1-\alpha)$, respectively, are required. To detect process deterioration the TBE is monitored and if it falls below the LCL, the process is declared out of control and an inspection takes place to determine assignable causes. Then monitoring resumes after the causes have been identified and removed or the out-of-control signal is deemed to be due to chance causes. A similar procedure is followed for the other cases.

To assess the performance of the control chart, we shall use the average run length (ARL) and the average length of inspection (ALI). The ARL is the number of points that, on average, will be plotted on the control chart until an out-of-control signal appears, i.e., for in-control situation $ARL = 1/\alpha$ while for out-of-control situation, it is $ARL = 1/(1-\zeta)$ where ζ denotes the type-II error. The ALI is defined as the average time (or length) of inspection which one has to wait before getting an out-of-control signal and can be written as $ALI = ARL \times E(Z)$.

Because getting an explicit expression of the first passage time distribution and finding its quantiles is extremely difficult in non-exponential cases, we propose Algorithm 1 to compute control limits in general cases.

Algorithm 1 Control limits computation for the first passage distribution to a fixed critical threshold.

1: Select $p = 1$ or $p = 2$ for the Process ▷ where $p = 1$ - Cumulative, $p = 2$ - Independent
2: Choose parameters values to generate X and M from F_X and G_M
3: Fix K
4: **for** $i = 1$ to S **do** ▷ where S is large, e.g., 10^6
5: **do**
6: Sample X_j and M_j, $j \ge 1$
7: **if** $p == 1$ **then**
8: $R_j = \sum_{l=1}^{j} M_l$
9: **else**
10: $R_j = M_j$
11: **end if**
12: **while** $R_j < K$
13: $Z_i = \sum_{l=1}^{j} X_l$
14: **end for**
15: Compute the sample quantiles of Z_i to find the LCL and UCL, respectively.

Similarly, Algorithm 2 computes ARL.

The design of a control chart is often based on ARL, a large in-control ARL is ensured by design, but the variance of the run length distribution can be large. Thus, in such scenario, the coefficient of variation (CV) provides good insights beyond ARL. An advantage of the CV is that different control charts with close ARL can be compared. Moreover, it is a scale-free measure. As noticed by Ali and Pievatolo [19], ALI is not a scale-free measure; therefore, we shall report only the CV values of the length of inspection (called CVLI).

In addition to these performance measures of the control charts, the quartiles of the run length distribution are also studied in detail. We

Algorithm 2 ARL Computation for the two-sided chart based on the renewal reward process with a fixed critical hreshold.

```
Select p = 1 or p = 2 for the Process        ▷ where p = 1 - Cumulative, p = 2 - Independent
Choose shifted parameters values to generate X and M from F_X and G_M
Fix K
for h = 1 to S do                            ▷ where S is large, e.g., 10^6
    i = 0
    do
        i = i + 1
        do
            Sample X_j and M_j, j ≥ 1
            if p == 1 then
                R_j = Σ_{l=1}^{j} M_l
            else
                R_j = M_j
            end if
        while R_j < K
        Z_i = Σ_{l=1}^{j} X_l
    while Z_i ≥ LCL || Z_i ≤ UCL
    RL_h = i, break
end for
Compute Mean of RL_h.
```

discuss the detection of process deterioration and improvement using the one and the two sided control charts, in the following subsections.

3.1. Adjusted values of parameters

Before presenting the simulation study of the ARL, is worthwhile to remark that a similar change in the ARL could be determined by a shift in either the time or the magnitude distribution. To demonstrate it for the cumulative process, let us suppose that θ_0 and λ_0 are the in-control rate parameters of a compound Poisson process and let us denote the mean of the first passage distribution by $z(\theta_0, \lambda_0) = (\theta_0 K + 1)/\lambda_0$ (see Example #1). Now consider a shift to θ_1, while λ stays at λ_0 and let us look for the corresponding shifted λ_1 while θ stays at θ_0. This is obtained by equating $z(\theta_1, \lambda_0)$ to $z(\theta_0, \lambda_1)$ which would result into $\lambda_1 = \frac{\theta_0 K+1}{z(\theta_1,\lambda_0)} = \frac{\lambda_0(\theta_0 K+1)}{\theta_1 K+1}$.

For example, take in-control rate parameters of the time and magnitude $\lambda_0 = 0.0005$ and $\theta_0 = 0.001$, respectively. If $\theta_1 = 0.003$ for $K = 300$, $\lambda_1 = 0.000342$. Similarly, θ_1 is found from λ_1 as $\theta_1 = \frac{\lambda_0 z(\theta_0,\lambda_1)-1}{K} = \frac{\lambda_0(\theta_0 K+1)-\lambda_1}{\lambda_1 K}$.

To find the shifted/adjusted parameter value in the independent process, we have $\theta_1 = \frac{\ln(\lambda_0)+\theta_0 K-\ln(\lambda_1)}{K}$, i.e., by using the λ_1, and $\lambda_1 = \lambda_0 \exp\{K(\theta_0 - \theta_1)\}$ for θ_1.

3.2. Discussion of an ARL study (cumulative process)

The performance of the charts has been evaluated for shifts in a wide range. This is because in practice the actual shift size is unknown. We considered shifts for the following two cases in the framework of the compound Poisson process of Section 2.3:

A λ decreases from $\lambda_0 = 0.0005$ to $\lambda_1 \in \{0.0003, 0.0001, 0.00005\}$ while θ increases from $\theta_0 = 0.001$ to $\theta_1 \in \{0.005, 0.002, 0.01\}$.
B λ increases from $\lambda_0 = 0.0005$ to $\lambda_1 \in \{0.005, 0.01, 0.1\}$ and θ decreases from $\theta_0 = 0.001$ to $\theta_1 \in \{0.00001, 0.0005, 0.0001\}$.

When the process is in-control, the ARL values of the one and the two sided charts are equal to the specified in-control ARL value, i.e., 370.

Case A: an increase in θ (or decrease in λ): In this case, to detect process improvement, the Upper-sided control chart has been employed and further it has been compared with the two-sided chart. We have computed the ARL and the CV of the run-length distribution and the length of inspection, for the two-sided and the upper-sided charts in Table 1. The standard deviation of the ARL can easily be recovered using the ARL and the CV values.

Table 1 shows some interesting results. By examining the ARL values, it is evident that the one-sided chart detects the shifts more effectively than the two-sided control chart, because the latter is more conservative by construction. This effectiveness is confirmed by the value of the CVs. The ARL values show a decreasing pattern as the shift in the rate parameter of the magnitude distribution occurs, therefore the charts are unbiased. The CV of the run length distribution is smaller and it decreases faster than the CV of the length of inspection as the process improves, confirming that the distribution of the length of inspection is more dispersed than distribution of the run length. The quartiles of the run-length distribution have also been computed (see Table A.1 in the appendix), and we noticed that as the shift in the rate parameter gets larger, the run length distribution becomes highly skewed and mean of the run length gets greater than Q_3. However, for small to moderate shifts, either in the rate parameter of the magnitude or time distribution, the ARL is between Q_2 and Q_3. Thus, runs rules to study the ARL performance may not be effective in such highly skewed distribution.

Case B: a decrease in θ (or an increase in λ): This is the most important case for a reliability engineer, because the parameter shifts are in the direction of process deterioration, for which the lower-sided control chart is well suited. Therefore, we compare the ARL and the CV values of the lower and the two sided control charts in Table 2.

Table 2 shows that the lower-sided chart is more efficient in the detection of process deterioration than the two-sided chart (again, the two-sided chart is more conservative). As the shift in the rate parameter of the time distribution occurs, the ARL and the CV get smaller. A shift of large size (either in the magnitude or time distribution) can be detected quickly as compared to a small shift. When the time distribution is in-control, i.e., $\lambda = \lambda_0$, but have a shift in the magnitude, i.e., $\theta < \theta_0$, then for the two-sided chart, we observe a reverse behavior of the ARL as compared to the process improvement case. Here, the ARL is clearly biased. However, the lower-sided chart is free from such shortcomings, and we advocate its superiority over the two-sided chart. Again, in this case, the CV values of the run length are smaller than the CV of the length of inspection, and both CVs support the superiority of the one-sided chart over the two-sided chart. We have also computed the quartiles in the appendix (cf. Table A.2), and observed that ARL value was smaller than Q_3. Therefore, the run length distribution is not as highly skewed as we observed in the case of process improvement.

3.3. Discussion of an ARL study (independent process)

Still using the model of Section 2.3, we consider shifts for the following two cases:

A λ decreases from $\lambda_0 = 0.0005$ to $\lambda_1 \in \{0.0003, 0.0001, 0.00005\}$ while θ increases from $\theta_0 = 0.001$ to $\theta_1 \in \{0.005, 0.002, 0.01\}$.
B λ increases from $\lambda_0 = 0.0005$ to $\lambda_1 \in \{0.005, 0.01, 0.1\}$ and θ decreases from $\theta_0 = 0.001$ to $\theta_1 \in \{0.00001, 0.0005, 0.0001\}$.

When the process is in-control, the ARL is equal to the specified in-control ARL value, i.e., 370.

Case A: an increase in θ (or decrease in λ): As in the Case A for the cumulative damage process, we consider the upper sided and the two sided charts for the detection of process improvement. From Table 3, it is clear that the one-sided chart is more efficient in the detection of shifts than the two-sided chart. The CV of the run-length also supports the superiority of the upper-sided control chart. The large-size shifts either in the rate parameter of the time or of the magnitude can be detected quickly as compared to the small shifts. The ARL gradually decreases with the shift in the parameters, so the charts are unbiased. The CV of the length of inspection distribution is constant so it is not useful. However,

Table 1
Process improvement with upper and two-sided charts for the cumulative damage process. The ARL is based on $\alpha = 0.0027$, $\lambda_0 = 0.0005, \theta_0 = 0.001$ and $\lambda_1 \in \{0.0003, 0.0001, 0.00005\}$, $\theta_1 \in \{0.002, 0.005, 0.01\}$.

θ	λ	Upper-sided				Two-sided			
		0.0005	0.0003	0.0001	0.00005	0.0005	0.0003	0.0001	0.00005
0.001	ARL	370.37	32.0474	3.05326	1.73591	370.37	46.1792	3.46456	1.84701
	CV	0.998649	0.984274	0.820049	0.651102	0.998649	0.989113	0.843424	0.67719
	CVLI	0.999928	0.999169	0.991241	0.984541	0.999928	0.999423	0.992285	0.985478
0.002	ARL	160.761	17.9681	2.40352	1.52591	231.902	25.2764	2.66728	1.60262
	CV	0.996885	0.971775	0.764162	0.587072	0.997842	0.980019	0.790624	0.613205
	CVLI	0.999563	0.996079	0.970305	0.952807	0.999697	0.997214	0.973282	0.955119
0.005	ARL	35.3429	6.41082	1.58941	1.22365	57.4729	8.37106	1.69522	1.25651
	CV	0.985751	0.918702	0.608964	0.42752	0.991262	0.938371	0.640394	0.451823
	CVLI	0.994894	0.971517	0.879489	0.840118	0.996863	0.978261	0.88749	0.844684
0.01	ARL	8.95931	2.69559	1.19192	1.06527	13.0939	3.2243	1.22946	1.07618
	CV	0.942541	0.79311	0.401274	0.247524	0.961056	0.830575	0.432009	0.266064
	CVLI	0.968099	0.889565	0.726687	0.686996	0.978285	0.908594	0.736533	0.690883

Table 2
Process deterioration with lower and two-sided charts for the cumulative damage process. The ARL is based on $\alpha = 0.0027$, $\lambda_0 = 0.0005, \theta_0 = 0.001$ and $\lambda_1 \in \{0.005, 0.01, 0.1\}$, $\theta_1 \in \{0.00001, 0.0001, 0.0005\}$ for lower and two-sided cumulative process charts.

θ	λ	Lower-sided				Two-sided			
		0.0005	0.005	0.01	0.1	0.0005	0.005	0.01	0.1
0.00001	ARL	275.351	27.9881	14.2486	1.93436	474.139	55.5067	28.0056	3.28049
	CV	0.998182	0.981973	0.96427	0.695006	0.998945	0.990951	0.981984	0.833767
	CVLI	1.0000	1.0000	1.0000	0.999998	1.0000	1.0000	1.0000	0.999999
0.0001	ARL	282.872	28.74	14.6243	1.97018	470.16	57.0118	28.758	3.35473
	CV	0.998231	0.982449	0.965205	0.701735	0.998936	0.991191	0.98246	0.837803
	CVLI	0.999999	0.999985	0.999971	0.999785	0.999999	0.999993	0.999985	0.999874
0.0005	ARL	318.868	32.3338	16.4177	2.13813	436.744	64.2106	32.3542	3.70586
	CV	0.998431	0.984415	0.969067	0.72959	0.998855	0.992183	0.984425	0.854492
	CVLI	0.999973	0.999737	0.999482	0.996014	0.999981	0.999868	0.999737	0.997702
0.001	ARL	370.37	37.4646	18.9721	2.36971	370.37	74.5005	37.4882	4.19766
	CV	0.998649	0.986564	0.973289	0.760268	0.998649	0.993266	0.986572	0.872795
	CVLI	0.999928	0.999289	0.998596	0.9887	0.999928	0.999643	0.999289	0.993636

Table 3
Process improvement with upper and two-sided charts for the independent damage process. The ARL is based on $\alpha = 0.0027$, $\lambda_0 = 0.0005, \theta_0 = 0.001$ and $\lambda_1 \in \{0.0003, 0.0001\ , 0.00005\}$, $\theta_1 \in \{0.002, 0.005, 0.01\}$.

θ	λ	Upper-sided				Two-sided			
		0.0005	0.0003	0.0001	0.00005	0.0005	0.0003	0.0001	0.00005
0.001	ARL	370.37	34.7682	3.26383	1.80661	370.37	50.5407	3.74536	1.93577
	CV	0.998649	0.985514	0.832833	0.668189	0.998649	0.990058	0.856156	0.695276
	CVLI	1.0000	1.0000	1.0000	1.0000	1.0000	1.0000	1.0000	1.0000
0.002	ARL	79.9636	13.8591	2.40203	1.54985	117.873	18.6488	2.66041	1.63125
	CV	0.993727	0.963247	0.763993	0.59563	0.995749	0.972819	0.790012	0.62207
	CVLI	1.0000	1.0000	1.0000	1.0000	1.0000	1.0000	1.0000	1.0000
0.005	ARL	5.93825	2.91202	1.42801	1.19499	7.29518	3.29797	1.48872	1.22014
	CV	0.911921	0.810306	0.547472	0.40395	0.928937	0.834735	0.572959	0.424764
	CVLI	1.0000	1.0000	1.0000	1.0000	1.0000	1.0000	1.0000	1.0000
0.01	ARL	1.48808	1.26933	1.08274	1.04055	1.55882	1.30522	1.09286	1.0454
	CV	0.572707	0.460636	0.276441	0.197406	0.59874	0.483576	0.29149	0.20839
	CVLI	1.0000	1.0000	1.0000	1.0000	1.0000	1.0000	1.0000	1.0000

the CV of the run of length distribution supports the superiority of the upper-sided chart. It is observed from the quartiles table (cf. Table A.3), given in the appendix, that a very large shift either in a damage or time will result into a highly skewed distribution of the run-length, i.e., ARL will be greater than Q_3. However, for small to moderate shifts, the ARL lies between Q_2 and Q_3.

Case B: a decrease in θ (or an increase in λ)**:** This case is more important because shifts in the parameters are in the direction of a process deterioration. As in the previous Case B we compare the lower-sided and the two-sided control chart in Table 4.

By examining Table 4 we noticed that the lower-sided chart is more efficient in the detection of process deterioration than the two-sided chart. We observe that the ARL of the two-sided chart is biased as compared to the lower-sided chart, especially when a shift is only in the rate parameter of the magnitude distribution. However, if we fix the damage distribution and introduce a shift in the rate parameter of the time distribution, then the ARL values get small, i.e., the control chart detection ability improves. A shift of large size either in time or damage will be detected quickly as compared to the small shift. The CV of the run length distribution supports the effectiveness of the lower-sided chart whereas the CV of the length of inspection distribution is not too informative. We also computed the quartiles of the run-length distribution in the appendix (cf. Table A.4) and found that the ARL values lie between the median and Q_3, which means that the run-length distribution is not highly skewed as we have observed in the case of process improvement.

Table 4
Process deterioration with lower and two-sided charts for the independent damage process. ARL based on $\alpha = 0.0027$, $\lambda_0 = 0.0005, \theta_0 = 0.001$ and $\lambda_1 \in \{0.005, 0.01, 0.1\}$, $\theta_1 \in \{0.00001, 0.0005, 0.0001\}$.

θ	λ	Lower-sided				Two-sided			
		0.0005	0.005	0.01	0.1	0.0005	0.005	0.01	0.1
0.00001	ARL	275.33	27.986	14.2476	1.93426	511.818	55.5047	28.0046	3.28039
	CV	0.998182	0.981971	0.964268	0.694987	0.999023	0.990951	0.981983	0.833762
	CVLI	1.0000	1.0000	1.0000	1.0000	1.0000	1.0000	1.0000	1.0000
0.0001	ARL	282.852	28.7381	14.6235	1.9703	514.881	57.0099	28.7572	3.35486
	CV	0.998231	0.982447	0.965203	0.701757	0.999028	0.991191	0.982459	0.837809
	CVLI	1.0000	1.0000	1.0000	1.0000	1.0000	1.0000	1.0000	1.0000
0.0005	ARL	318.85	32.3376	16.4227	2.14376	492.206	64.2144	32.3592	3.71177
	CV	0.998431	0.984417	0.969076	0.730432	0.998984	0.992183	0.984427	0.854744
	CVLI	1.0000	1.0000	1.0000	1.0000	1.0000	1.0000	1.0000	1.0000
0.001	ARL	370.37	37.4893	18.998	2.39419	370.37	74.5252	37.5143	4.22369
	CV	0.998649	0.986573	0.973326	0.763101	0.998649	0.993268	0.986582	0.873636
	CVLI	1.0000	1.0000	1.0000	1.0000	1.0000	1.0000	1.0000	1.0000

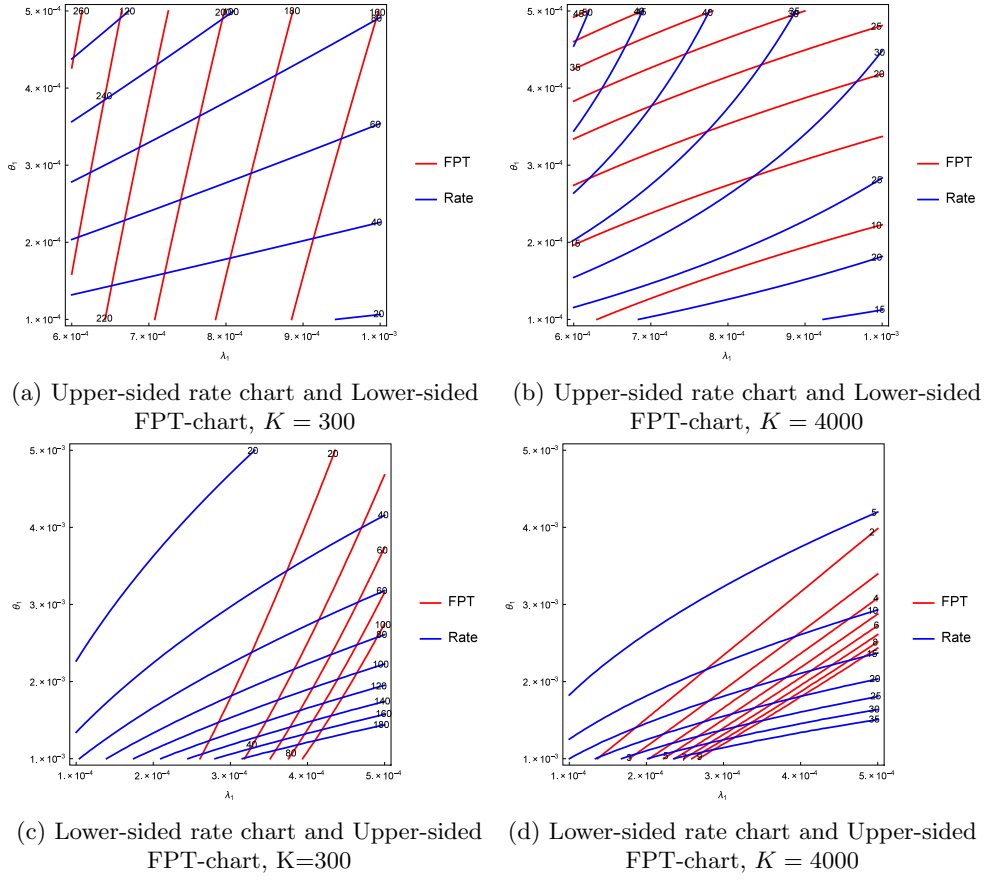

(a) Upper-sided rate chart and Lower-sided FPT-chart, $K = 300$

(b) Upper-sided rate chart and Lower-sided FPT-chart, $K = 4000$

(c) Lower-sided rate chart and Upper-sided FPT-chart, K=300

(d) Lower-sided rate chart and Upper-sided FPT-chart, $K = 4000$

Fig. 3. Comparison of the ARL of the FPT and rate control charts for the cumulative damage process. Panels (a) and (b): process deterioration; panels (c) and (d): process improvement. The ARL of the rate chart has been scaled.

3.4. A comparison between FPT and rate charts

In this section, we compare the FPT-charts to the rate charts on the basis of the ARL. In Fig. 3, we have depicted the level curves of the ARL of one and two-sided charts using thresholds $K = 300$ or $K = 4000$ for the cumulative damage process under the compound Poisson process assumption. For process deterioration, the lower sided FPT-chart is compared to the upper-sided rate chart, whereas for process improvement the reverse is done. The rate charts are built from pairs (X_i, M_i) and they monitor M_i/X_i (cf. Appendix B), so, for every monitored point on the FPT-chart, the number of arrivals needed to cross the threshold are monitored on the rate chart. Therefore, to make the comparison valid, the ARL of the rate chart was divided by the expected number of these arrivals, $(\theta_1 K + 1)$ (derived from $E(Z)$ in Example #1 and Wald's equation). When K is smaller, the FPT-chart is better at detecting process improvement; as K gets larger then it can outperform the rate chart also at detecting process deterioration. The reason why the rate chart does better in Fig. 3(a) is that the FPT-chart is insensitive to θ_1 in the selected range, because for K in the hundreds the threshold is very often crossed at the first arrival and so the stopping time depends mainly on the inter-arrival times (governed by λ_1) and the information on the magnitude is unused, whereas the rate chart uses it effectively. However, as K gets larger (representing a system with a longer lifetime), the FPT-chart starts to use the information on magnitude and the performance improves.

In Fig. 4, the same analysis is presented for the independent damage process, but dividing the ARL of the rate process by $\exp(\theta_1 K)$ (see Ex-

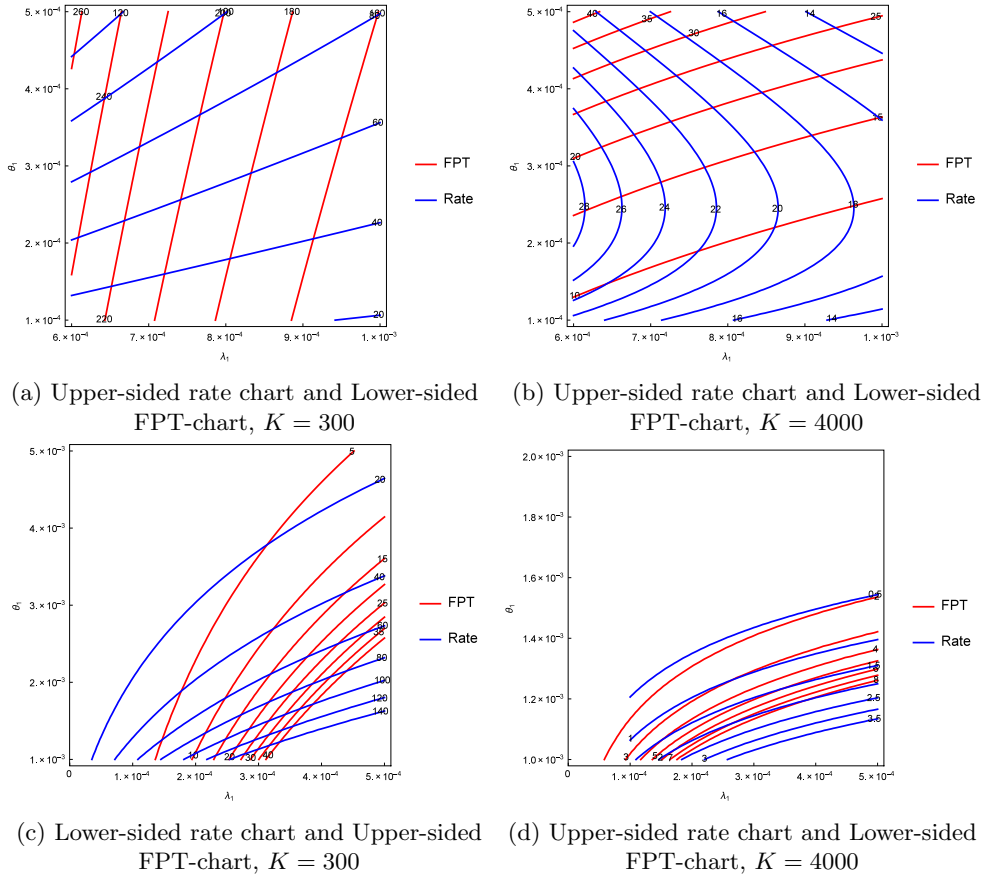

(a) Upper-sided rate chart and Lower-sided FPT-chart, $K = 300$

(b) Upper-sided rate chart and Lower-sided FPT-chart, $K = 4000$

(c) Lower-sided rate chart and Upper-sided FPT-chart, $K = 300$

(d) Upper-sided rate chart and Lower-sided FPT-chart, $K = 4000$

Fig. 4. Comparison of the ARL of FPT and rate control charts for the independent damage process. Panels (a) and (b): process deterioration; panels (c) and (d): process improvement. The ARL of the rate chart has been scaled.

ample #2), and we reach similar conclusions for $K = 300$. Instead, for $K = 4000$, Fig. 4(b) indicates that no chart dominates the other on the selected range, but the FPT-chart is more sensitive to larger deteriorations (large λ_1 and in particular small θ_1). Finally, in Fig. 4(c) the rate chart is slightly more effective, but the ARL is very small for both charts.

4. Real life examples

In this section, we discuss some illustrative real-life examples with simulated data sets for the implementation of the proposed control charts. We have used $\alpha = 0.0027$ as false alarm probability.

4.1. Wire rope strength monitoring-cumulative process

Wire ropes of a properly designed and maintained crane will deteriorate throughout their entire service life by two principal deterioration mechanisms, which are: external and internal fatigue, caused by bending over sheaves or winding on drums, and crushing caused by spooling on multilayered drums (cf. Weischedel [20]). An experiment is designed to test the compatibility of wire rope with two different sheaves/winding on drums. A dataset of the damage of a wire rope is collected and given in Table 5. The dataset was built by assuming that every time a weight is lifted, the damage to wires is measured by electromagnetic inspection and weights continue to be lifted until the cumulative damage crosses a specified threshold. The first 20 in-control observations as given in Table 5 were generated using $\lambda = 0.0005, \theta = 0.001$, and the next 10 (i.e., a new model of the sheave was introduced for testing the wire compatibility) from $\lambda = 0.0001, \theta = 0.001$. Similarly, the last 10 (that is, a second model of the sheave was introduced for testing wire compatibility) from $\lambda = 0.01, \theta = 0.001$. Boldface numbers denote the occurrence

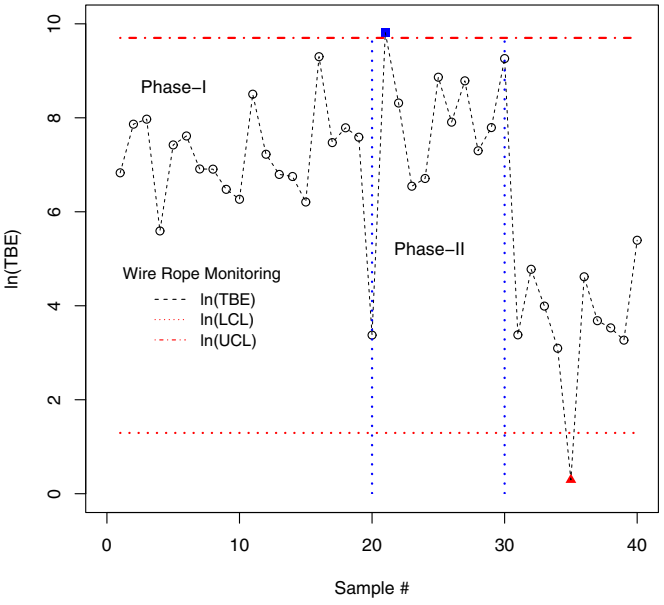

Fig. 5. Control chart for the cumulative process monitoring.

of the shift, while values marked with ⋆ represent the detection of the shift, i.e., a signal of the compatibility of the sheave with wire rope, by the control chart. Using the first 20 observations, the control limits are $LCL = \ln(3.64695) = 1.293891$ and $UCL = \ln(16321.1) = 9.700214$. In Fig. 5, the natural logarithm of the data and of the control limits are

Table 5
Simulated failure time data of the cumulative process.

Failure #	Inter-failure time (X)	ln (*X*)	Cumulative Probability	Failure #	Inter-failure time (X)	ln (*X*)	Cumulative Probability
1	924.377	6.8291	0.2921	21	18283.98	**9.8138**⋆	0.9994
2	2601.66	7.8639	0.6270	22	4082.99	8.3146	0.7908
3	2895.77	7.9710	0.6671	23	695.201	6.5442	0.2284
4	268.329	5.5922	0.0949	24	819.318	6.7085	0.2636
5	1672.99	7.4224	0.4671	25	7070.88	8.8637	0.9366
6	2024.72	7.6132	0.6342	26	2716.55	7.9071	0.6432
7	1002.97	6.9107	0.3128	27	6546.95	8.7868	0.9216
8	999.332	6.9071	0.3118	28	1478.42	7.2987	0.4261
9	650.125	6.4772	0.2152	29	2421.04	7.7919	0.6001
10	526.436	6.2661	0.1780	30	10508.8	9.2599	0.9845
11	4926.25	8.5023	0.8501	31	29.3991	**3.3809**	0.0108
12	1372.49	7.2244	0.4025	32	118.681	4.7764	0.0431
13	892.819	6.7944	0.2836	33	54.1987	3.9927	0.0199
14	854.872	6.7509	0.2733	34	22.09	3.0951	0.0082
15	496.659	6.2079	0.1687	35	1.3452	0.2965⋆	0.0004
16	10943.1	9.3005	0.9870	36	101.146	4.6166	0.0368
17	1759.06	7.4725	0.4843	37	39.7277	3.6821	0.0146
18	2409.34	7.7871	0.5982	38	34.1069	3.5295	0.0126
19	1972.39	7.5870	0.5248	39	26.2636	3.2682	0.0097
20	29.2355	3.3754	0.0108	40	220.035	5.3938	0.0784

Table 6
Simulated failure time data of the independent process.

Failure #	Inter-failure time (X)	ln (*X*)	CP	Failure #	Inter-failure time (X)	ln (*X*)	CP
1	28.1469	3.3374	0.0104	21	1.6689	**0.5122**⋆	**0.0006**⋆
2	5375.9799	8.5897	0.8635	22	38.7736	3.6577	0.0143
3	4899.0753	8.4968	0.8371	23	30.4048	3.4146	0.0112
4	326.0282	5.7869	0.1138	24	6.0719	1.8037	0.0023
5	3792.8213	8.2409	0.7546	25	7.2365	1.9791	0.0027
6	468.8966	6.1504	0.1594	26	1.6809	0.5193⋆	0.0006⋆
7	7043.6737	8.8599	0.9264	27	9.3069	2.2308	0.0034
8	8111.0884	9.0009	0.9504	28	14.0128	2.6399	0.0052
9	1824.1795	7.5089	0.4912	29	8.7200	2.1656	0.0032
10	524.2249	6.2619	0.1765	30	4.8538	1.5798	0.0018
11	5259.7901	8.5679	0.8575	31	2710.1264	**7.9048**	**0.6335**
12	1500.3225	7.3134	0.4264	32	4673.8559	8.4497	0.8229
13	2280.1749	7.7320	0.5703	33	834.6655	6.7270	0.2659
14	1772.6952	7.4803	0.4814	34	91.5559	4.5169	0.0334
15	2828.1483	7.9474	0.6492	35	13853.8589	9.5363	0.9941
16	2570.5627	7.8519	0.6141	36	33313.4361	10.4137⋆	0.9999⋆
17	498.3389	6.2113	0.1686	37	1697.9908	7.4372	0.4669
18	3595.0558	8.1873	0.7359	38	418.0323	6.0356	0.1435
19	2743.4973	7.9169	0.6380	39	33.6614	3.5164	0.0124
20	1489.9068	7.3065	0.4241	40	2546.4320	7.8425	0.6106

shown for a better presentation of the chart. From Table 5 or Fig. 5, clearly, the first model of the sheave is more compatible with the wire rope than the second one. Moreover, this conclusion is in accordance with the simulation study (cf Section 3).

4.2. Water quality monitoring-independent process

There are environmental protocols which must be followed and ensured by each factory before releasing wastage. If a factory leaks poisonous waste products into a river, the vegetation and the fish in the river may die due to the effect of a cumulative or of an accidental massive poison pouring. To differentiate between an accidental and intentional poisoning of a river, we propose an independent process to monitor water quality.

Conductivity of the water can be used to check water quality, because it depends on the concentration of dissolved electrolyte ions in the water. Every creek will have a baseline conductivity depending on the local geology and soils. Higher conductivity will result from the presence of various ions, including nitrate, phosphate, and sodium. Conductivity can be measured in Siemens per centimeter (S/cm). Distilled water has a conductivity ranging from 0.5 to 3 μS/cm, while most streams range between 50 to 1500 μS/cm. Freshwater streams ideally should have a conductivity between 150 to 500 μS/cm to support diverse aquatic life.

Let us suppose that conductivity should be at most 300 μS/cm for a particular river or stream which is near a factory. Forty observations have been generated in Table 6 to check the stream water quality where data are the hours between crossings of the conductivity threshold. The first 20 in-control observations (cf. Table 6) were generated using $K = 300, \lambda = 0.0005, \theta = 0.001$, the next 10, to represent process deterioration, from $\lambda = 0.1, \theta = 0.0001$ and the last 10, i.e., process improvement, from $\lambda = 0.0001, \theta = 0.001$. The bold values in Table 6 denote the occurrence of a shift while values with a ⋆ represent the detection of the shift by the FPT-chart. Using the first 20 observations, the control limits are $LCL = \ln(3.64708) = 1.293927$ and $UCL = \ln(17838.8) = 9.789131$. Note that process improvement means that conductivity is decreasing, while process deterioration means that conductivity is increasing. In Fig. 6, the natural logarithm of the data and of the control limits are taken for a better presentation of the chart. From Fig. 6, clearly, the process is in-control for the first 20 observations. A shift of the process deterioration occurred at sample number 21, and it was immediately detected by the chart. Similarly, another shift occurred at sample number 31 which was detected at sample number 36.

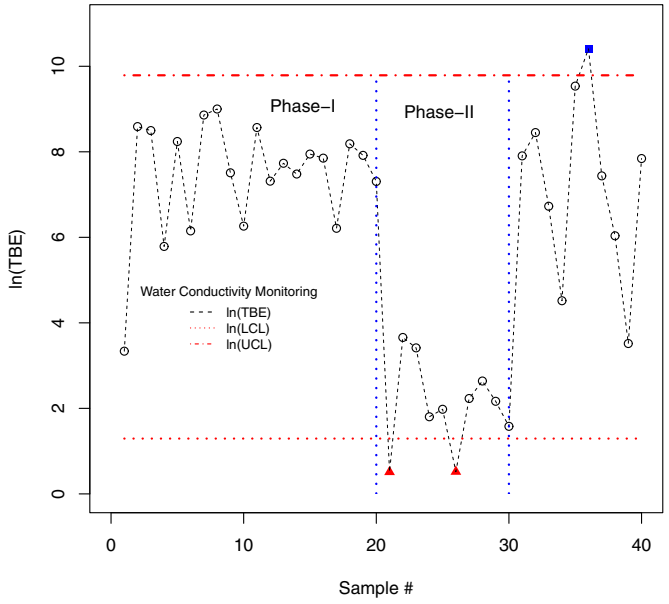

Fig. 6. FPT chart for the independent damage process monitoring.

5. Conclusion

In this article we have proposed the FPT-chart, a control chart based on the monitoring of first passage times above a threshold. This chart is useful to monitor sequences of times between substitutions of a product or of a piece of equipment due to failure or damage (regarded as first passage times) . A change in the distribution of first passage times may signal usage beyond design limits or other permanent deficiencies that were inadvertently introduced in the product or process, degrading its reliability. The FPT-chart assumes that the underlying damage process is a shock process, where shocks occur following a renewal process with rewards, representing the magnitude of the shocks.

There is a relationship with the existing literature on the joint monitoring of time and magnitude, in which the marked Poisson process is commonly used. The FPT-charts are not a direct generalisation of the time and magnitude charts, however they constitute an advancement in several respect: they are built under the assumption of a more general underlying stochastic process; they can be a substitute for the rate charts, by which proportional changes of time and magnitude would go undetected; they can be used when the magnitude of the damage is not observable, which is not possible for the time and magnitude charts; like the time and magnitude charts, they are en extension, in another direction, of the simple TBE charts; they can be more effective than the time and magnitude charts in the detection of out-of-control situations, as shown by a numerical study on the ARL in the case of a compound Poisson process.

An advantage of the renewal reward process is that it allows for any distribution of the TBE and of the magnitude. A drawback is that there are not general closed form expressions for the calculation of control limits. We have proposed simple Monte Carlo algorithms to compute the control limits and the ARL, however, when reliability is very high, the simulation of first passage times can be very time consuming and very long runs may be required to reduce the Monte Carlo variance to acceptable values. So, while we have used Monte Carlo simulation effectively in this study, there is the need for developing specialised numerical method for the computation of quantiles of first passage time distributions available from renewal theory, with a view to actual applications of the FPT-charts. Other possible developments are the study of the effect of parameter estimation on FPT-charts (and, more generally, on charts for the monitoring of time and magnitude) and the relaxation of the assumption of independence of magnitude from time.

Acknowledgments

The first author presented this work at the 4th Symposium on Games and Decisions in Reliability and Risk (GDRR), June 17–19, 2015, Istanbul, Turkey. He acknowledges the travel support provided by the Fondazione Cariplo Mobility Fund to attend GDRR 2015. The first author acknowledges the excellent research facilities available at Bocconi University, and especially would also like to thank Professor Sonia Petrone (Department of Decision Sciences, Bocconi University, Milan, Italy) for her valuable comments and support.

The authors would like to thank the anonymous referees, Editor and especially the Guest Editor for helpful and valuable comments and suggestions that have resulted in significant improvements in the quality of this article.

Appendix A

Quartiles of the run-length distribution for the cumulative and independent processes are given in Tables A.1, A.2, A.3, and A.4.

Appendix B

To compare the FPT-chart and the rate chart, we derived the cumulative probability function of the random variable $R = M/X$ as follows: $F_r(R) = P(R \le r) = P\left(\frac{M}{X} \le r\right) = \int_0^\infty P\left(X \ge \frac{M}{r} | M\right) f(M) dM = \int_0^\infty \exp\left(\frac{-\lambda M}{r}\right) \theta \exp(-\theta M) dM = \frac{r\theta}{\lambda + r\theta}$. Then $LCL = F^{-1}(\alpha)$ and $UCL = F^{-1}(1-\alpha)$. To detect deterioration we used the upper-sided rate chart and the lower-sided FPT-chart. Similarly, to detect improvement we used the lower-sided rate chart and the upper-sided FPT-chart.

Table A.1
Quartiles of the run-length distribution based on $\alpha = 0.0027, \lambda_0 = 0.0005, \theta_0 = 0.001$ and $\lambda_1 \in \{0.0003, 0.0001, 0.00005\}$, $\theta_1 \in \{0.005, 0.002, 0.01\}$ for the upper and two-sided cumulative process charts.

θ	λ	Upper-sided				Two-sided			
		0.0005	0.0003	0.0001	0.00005	0.0005	0.0003	0.0001	0.00005
0.001	Q_1	106.405	9.07486	0.725039	0.335224	106.405	13.1406	0.844703	0.369009
	Q_2	256.374	21.8652	1.74692	0.807696	256.374	31.6612	2.03525	0.889097
	Q_3	512.749	43.7303	3.49385	1.61539	512.749	63.3223	4.07049	1.77819
0.002	Q_1	46.1041	5.02389	0.534773	0.27007	66.57	7.12675	0.612266	0.29412
	Q_2	111.084	12.1047	1.28849	0.650711	160.395	17.1713	1.47521	0.708659
	Q_3	222.169	24.2093	2.57699	1.30142	320.79	34.3427	2.95041	1.41732
0.005	Q_1	10.023	1.69637	0.290004	0.169273	16.3897	2.26131	0.322751	0.181054
	Q_2	24.1496	4.08728	0.698742	0.407851	39.4896	5.44845	0.777643	0.436235
	Q_3	48.2992	8.17455	1.39748	0.815702	78.9791	10.8969	1.55529	0.87247
0.01	Q_1	2.43076	0.620557	0.157529	0.10302	3.62113	0.774853	0.17138	0.10864
	Q_2	5.85671	1.49518	0.379553	0.248218	8.72482	1.86695	0.412928	0.261759
	Q_3	11.7134	2.99037	0.759106	0.496436	17.4496	3.73389	0.825855	0.523518

Table A.2
Quartiles of the run-length distribution based on $\alpha = 0.0027, \lambda_0 = 0.0005, \theta_0 = 0.001$ and $\lambda_1 \in \{0.005, 0.01, 0.1\}$, $\theta_1 \in \{0.00001, 0.0001, 0.0005\}$ for the lower and two-sided cumulative process charts.

θ	λ	Lower-sided				Two-sided			
		0.0005	0.005	0.01	0.1	0.0005	0.005	0.01	0.1
0.00001	Q_1	79.0695	7.90695	3.95347	0.395347	136.257	15.824	7.912	0.7912
	Q_2	190.512	19.0512	9.52558	0.952557	328.301	38.1267	19.0633	1.90633
	Q_3	381.023	38.1023	19.0512	1.90511	656.602	76.2534	38.1267	3.81267
0.0001	Q_1	81.2334	8.12328	4.06161	0.406102	135.113	16.257	8.12847	0.812788
	Q_2	195.725	19.5724	9.78612	0.97847	325.543	39.17	19.5849	1.95835
	Q_3	391.451	39.1448	19.5722	1.95694	651.086	78.34	39.1698	3.9167
0.0005	Q_1	91.5887	9.15726	4.57774	0.456243	125.499	18.328	9.16312	0.914742
	Q_2	220.676	22.0637	11.0297	1.09928	302.381	44.1599	22.0778	2.204
	Q_3	441.351	44.1274	22.0594	2.19857	604.762	88.3198	44.1556	4.408
0.001	Q_1	106.405	10.6334	5.31279	0.524807	106.405	21.2883	10.6402	1.05723
	Q_2	256.374	25.6203	12.8008	1.26448	256.374	51.2924	25.6367	2.54732
	Q_3	512.749	51.2407	25.6015	2.52896	512.749	102.585	51.2735	5.09464

Table A.3
Quartiles of the run-length distribution based on $\alpha = 0.0027, \lambda_0 = 0.0005, \theta_0 = 0.001$ and $\lambda_1 \in \{0.0003, 0.0001, 0.00005\}$, $\theta_1 \in \{0.002, 0.005, 0.01\}$ for the upper and two-sided independent process charts.

θ	λ	Upper-sided				Two-sided			
		0.0005	0.0003	0.0001	0.00005	0.0005	0.0003	0.0001	0.00005
0.001	Q_1	106.405	9.85764	0.786353	0.356762	106.405	14.3953	0.926198	0.39577
	Q_2	256.374	23.7512	1.89465	0.85959	256.374	34.6844	2.2316	0.953576
	Q_3	512.749	47.5024	3.78931	1.71918	512.749	69.3689	4.4632	1.90715
0.002	Q_1	22.86	3.84138	0.534335	0.277613	33.766	5.21977	0.610252	0.303013
	Q_2	55.0793	9.25551	1.28744	0.668887	81.3565	12.5766	1.47035	0.730086
	Q_3	110.159	18.511	2.57487	1.33777	162.713	25.1532	2.94071	1.46017
0.005	Q_1	1.56007	0.683841	0.238762	0.158684	1.95132	0.796283	0.258269	0.167995
	Q_2	3.75886	1.64766	0.575279	0.382336	4.70155	1.91858	0.62228	0.404771
	Q_3	7.51772	3.29532	1.15056	0.764672	9.4031	3.83716	1.24456	0.809542
0.01	Q_1	0.258066	0.185566	0.111873	0.088654	0.280431	0.197979	0.116683	0.091715
	Q_2	0.62179	0.447107	0.269548	0.213606	0.675676	0.477014	0.281138	0.220981
	Q_3	1.24358	0.894213	0.539096	0.427211	1.35135	0.954029	0.562277	0.441961

Table A.4
Quartiles of the run-length distribution based on $\alpha = 0.0027, \lambda_0 = 0.0005, \theta_0 = 0.001$ and $\lambda_1 \in \{0.005, 0.01, 0.1\}$, $\theta_1 \in \{0.00001, 0.0001, 0.0005\}$ for the lower and two-sided Independent process charts.

θ	λ	Lower-sided				Two-sided			
		0.0005	0.005	0.01	0.1	0.0005	0.005	0.01	0.1
0.00001	Q_1	79.0636	7.90636	3.95318	0.395318	147.097	15.8234	7.91171	0.791171
	Q_2	190.497	19.0497	9.52487	0.952487	354.419	38.1253	19.0626	1.90626
	Q_3	380.995	38.0995	19.0497	1.90497	708.838	76.2505	38.1253	3.81253
0.0001	Q_1	81.2274	8.12274	4.06137	0.406137	147.978	16.2565	8.12823	0.812823
	Q_2	195.711	19.5711	9.78555	0.978555	356.541	39.1687	19.5843	1.95843
	Q_3	391.422	39.1422	19.5711	1.95711	713.083	78.3373	39.1687	3.91687
0.0005	Q_1	91.5836	9.15836	4.57918	0.457918	141.455	18.3291	9.16456	0.916456
	Q_2	220.664	22.0664	11.0332	1.10332	340.824	44.1626	22.0813	2.20813
	Q_3	441.327	44.1327	22.0664	2.20664	681.649	88.3251	44.1626	4.41626
0.001	Q_1	106.405	10.6405	5.32025	0.532025	106.405	21.2954	10.6477	1.06477
	Q_2	256.374	25.6374	12.8187	1.28187	256.374	51.3096	25.6548	2.56548
	Q_3	512.749	51.2749	25.6374	2.56374	512.749	102.619	51.3096	5.13096

References

[1] Montgomery DC. Introduction to the statistical quality control. John Wiley and Sons, New York; 2009.
[2] Woodall WH, Montgomery DC. Some current directions in the theory and application of statistical process control. J Quality Technol 2014;46:78–94.
[3] Wu Z, Jiao J, He Z. A control scheme for monitoring the frequency and magnitude of an event. Int J Product Res 2009;47:2887–902.
[4] Wu Z, Jiao J, He Z. A single control chart for monitoring the frequency and magnitude of an event. Int J Product Econ 2009;119:24–33.
[5] Liu Y, He Z, Shu L, Wu Z. Statistical computation and analysis for attribute events. Comput Stat Data Anal 2009;53:3412–25.
[6] Liu Y, He Z, Shamsuzzaman M, Wu Z. A combined control scheme for monitoring the frequency and size of an attribute event. J Appl Stat 2010;37:1991–2013.
[7] Qu L, Wu Z, Khoo MBC, Shu LJ. A new control chart for monitoring the event frequency and magnitude. Eu J Ind Eng 2014;8:789–813.
[8] Wu Z, Liu Y, He Z, Khoo MBC. A cumulative sum scheme for monitoring frequency and size of an event. Quality Reliab Eng Int 2010;26:541–54.
[9] Qu L, Wu Z, Khoo MBC, Castagliola P. A CUSUM scheme for event monitoring. Int J Product Econ 2013;145:268–80.
[10] Qu L, Wu Z, Rahim A, Khoo MBC. A balanced two-sided CUSUM chart for monitoring time between events. Eur J Ind Eng 2015;9:1–26.
[11] Ali S, Pievatolo A, Göb R. An overview of control charts for high quality processes. Quality Reliab Eng Int 2016;32:2171–89.
[12] Xie M, Goh T, Ranjan P. Some effective control chart procedures for reliability monitoring. Reliab Eng Syst Safety 2002;77:143–50.
[13] Vining G, Kulahci M, Pedersen S. Recent advances and future directions for quality engineering. Quality Reliab Eng Int 2015. doi:10.1002/qre.1797. iFirst.
[14] Gut A, Hüsler J. Advances in degradation modeling. In: Statistics for industry and technology, vol. 4982. Birkhäuser Boston, a part of Springer Science and Business Media, 2010; 2010. p. 59–76. chap. Shock Models.
[15] Nakagawa T. Maintenance theory of reliability. Springer-Verlag London; 2005.

[16] Nakagawa T. Shock and damage models in reliability theory. Springer-Verlag London; 2007.
[17] Barlow RE, Proschan F. Mathematical theory of reliability. Philadelphia, PA: Jhon Wiley and Sons; 1965. Reprinted (1996) SIAM.
[18] Graf U. Applied Laplace transforms and z-transforms for scientists and engineers. Springer Basel AG; 2004.
[19] Ali S, Pievatolo A. High quality process monitoring using a class of inter-arrival time distributions of the renewal process. Comput Ind Eng 2016;94:45–62.
[20] Weischedel HR. Crane wire rope damage and nondestructive inspection methods, 25. Wire Rope News and Sling Technology; 2003. p. 1–11.